

Convergence of hydrodynamics in a rotating strongly coupled plasma

Casey Cartwright^{*}


Department of Physics and Astronomy, University of Alabama, 514 University Boulevard, Tuscaloosa, Alabama 35487, USA and Institute for Theoretical Physics, Utrecht University, Princetonplein 5, 3584 CC Utrecht, The Netherlands

Markus Garbiso Amano[†] and Matthias Kaminski[‡]

Department of Physics and Astronomy, University of Alabama, 514 University Boulevard, Tuscaloosa, Alabama 35487, USA

Jorge Noronha[§] and Enrico Speranza^{||}

Illinois Center for Advanced Studies of the Universe, Department of Physics, University of Illinois at Urbana-Champaign, Urbana, Illinois 61801, USA

 (Received 3 February 2022; revised 28 April 2023; accepted 1 August 2023; published 18 August 2023)

We compute the radius of convergence of the linearized relativistic hydrodynamic expansion around a nontrivially rotating strongly coupled $\mathcal{N} = 4$ super-Yang-Mills plasma. Our results show that the validity of hydrodynamics is sustained and can even get enhanced for conformal field theory (CFT) in a rotating state. Analytic equations for the hydrodynamic dispersion relations and transport coefficients of the rotating plasma as a function of their values in a plasma at rest are given.

DOI: [10.1103/PhysRevD.108.046014](https://doi.org/10.1103/PhysRevD.108.046014)

I. INTRODUCTION

Relativistic hydrodynamics is a powerful tool to describe the late time, long wavelength behavior of the strongly coupled quark-gluon plasma (QGP) formed in ultrarelativistic heavy-ion collisions [1–3]. Recent experimental results show that certain hadrons (e.g. Lambda-hyperons) emitted in noncentral collisions exhibit nonzero spin polarization, which indicates that the QGP is the most vortical fluid observed to date [4]. Despite some early successes [5], a number of questions concerning the vorticity of the QGP still remain, see e.g. [5–21]. One crucial aspect yet to be understood is how the large angular momentum present at the early stages of the collision influences the emergence of hydrodynamics [22] in the presence of vorticity. A fundamental related question is then: what is the range of validity of hydrodynamics in a rapidly rotating strongly coupled QGP? This is a challenging mathematical problem to answer in a

general hydrodynamic or kinetic theory setting and is currently beyond the reach of standard first-principles approaches [23], as it requires knowledge about the real-time properties of QCD in the strongly coupled regime.

In this work we answer this question for a particular solution to a well-established “toy-model” of the rotating QGP, i.e., the strongly coupled $\mathcal{N} = 4$ super-Yang-Mills (SYM) plasma at nonzero temperature and angular momentum, using the gauge/gravity correspondence (holography) [24]. This model consists of a rotating plasma of quarks and gluons (in the adjoint representation) of $\mathcal{N} = 4$ SYM theory with gauge symmetry $SU(N_c)$ in the limit of an infinite number of colors, $N_c \rightarrow \infty$, and a large (’t Hooft) coupling constant λ . By investigating the critical points of spectral curves as developed in Refs. [25,26], we show that the radius of convergence of the hydrodynamic series, which quantifies the range of validity of the (linearized) hydrodynamic gradient expansion, remains finite at nonzero angular momentum. The radius of convergence can even increase for a sufficiently rapidly rotating plasma. Furthermore, we demonstrate, in an appropriate limit, that the transport coefficients of the rotating plasma can be explicitly obtained from their values in the plasma at rest.

II. HOLOGRAPHIC MODEL

In order to determine the values of hydrodynamic transport coefficients, we compute hydrodynamic modes and correlation functions of $\mathcal{N} = 4$ SYM plasma with

^{*}c.c.cartwright@uu.nl

[†]magarbiso@crimson.ua.edu

[‡]mski@ua.edu

[§]jn0508@illinois.edu

^{||}espera@illinois.edu

Published by the American Physical Society under the terms of the Creative Commons Attribution 4.0 International license. Further distribution of this work must maintain attribution to the author(s) and the published article’s title, journal citation, and DOI. Funded by SCOAP³.

the holographically dual Einstein gravity $S = 1/(16\pi G_5) \int d^5x \sqrt{-g}(\mathcal{R} - 2\Lambda)$, where \mathcal{R} is the Ricci scalar, G_5 is the five-dimensional gravitational Newton constant, and Λ the cosmological constant [27,28]. A rotating plasma is holographically dual to the rotating black hole metric which is asymptotic to AdS₅ spacetime [29,30]. In general, such a black hole is parametrized by two angular momenta, a and b , and it has the structure $\mathbb{R}_t \times \mathbb{R}_r \times S^3$ with a time coordinate $t \in (-\infty, \infty)$, the radial AdS coordinate $r \in (0, \infty)$, r_H being the event horizon radius, and the spatial 3-sphere S^3 parametrized by angles (θ, ϕ, ψ) . We set $b = a$ [31] and use a coordinate transformation (diffeomorphism) [16] yielding the rotating metric in the form [32–34]

$$ds^2 = -\left(1 + \frac{r^2}{L^2}\right) dt^2 + \frac{dr^2}{G(r)} + \frac{r^2}{4}((\sigma^1)^2 + (\sigma^2)^2 + (\sigma^3)^2) + \frac{2\mu}{r^2} \left(dt + \frac{a}{2}\sigma^3\right)^2$$

$$G(r) = 1 + \frac{r^2}{L^2} - \frac{2\mu(1 - a^2/L^2)}{r^2} + \frac{2\mu a^2}{r^4},$$

$$\mu = \frac{r_+^4(L^2 + r_+^2)}{2L^2 r_+^2 - 2a^2(L^2 + r_+^2)}, \quad (1)$$

with the radius of AdS, L , the AdS radial coordinate r , the horizon radius r_+ , the one-forms $\sigma^1, \sigma^2, \sigma^3$, which each are known covectors that depend on (θ, ϕ, ψ) [16]. Throughout this work we use natural units, $c = \hbar = k_B = 1$, and $G_5 = L^3 \pi / (2N_c^2)$. The solution in Eq. (1) will be referred to as the Myers-Perry (MP) black hole.

III. ROTATING EQUILIBRIUM STATE

In $\mathcal{N} = 4$ SYM theory, the rotating gravitational metric solution in the large black hole limit, keeping only the leading order in α

$$r_+ \rightarrow \alpha r_+, \quad r \rightarrow \alpha r, \quad \alpha \rightarrow \infty, \quad (2)$$

corresponds to a rotating conformal fluid solution of the ideal hydrodynamic equations of motion $\nabla_\mu T^{\mu\nu} = 0$, with total angular momentum of magnitude $J = a\pi\mu/G_5$ [35]. In Milne coordinates (τ, x_1, x_2, ξ) of flat Minkowski space [36], this flow can be written as

$$u^\tau = \lambda[\cosh \xi(L^2 + \tau^2 + x_\perp^2) + 2\Omega(Lx_1 \sinh \xi + \tau x_2)]$$

$$u^1 = \lambda[2(L\tau\Omega \sinh \xi + \tau x_1 \cosh \xi + x_1 x_2 \Omega)],$$

$$u^2 = \lambda[\Omega(L^2 + \tau^2 - x_1^2 + x_2^2) + 2\tau x_2 \cosh \xi], \quad (3)$$

$$u^\xi = -\tau^{-1} \lambda[-\sinh \xi(L^2 - \tau^2 + x_\perp^2) - 2Lx_1 \Omega \cosh \xi],$$

$$\epsilon = (16L^8 \Theta^4)(1 - \Omega^2)^{-2}(2L^2 \tau^2 \cosh 2\xi + (L^2 + x_\perp^2)^2 + \tau^4 - 2\tau^2 x_\perp^2)^{-2}, \quad (4)$$

$$\lambda = \left(\frac{\epsilon}{16L^8 \Theta^4}\right)^{1/4}, \quad \Theta = \left(\frac{3(1 - \Omega^2)\mu}{8\pi G_5 L^3}\right)^{1/4}, \quad (5)$$

where $\Omega = a/L$, $x_\perp^2 = x_1^2 + x_2^2$, $\tau = \sqrt{t^2 - x_3^2}$, $\xi = \text{arctanh}(x_3/t)$, and we recall that μ has dimensions L^2 and Θ carries units of energy because $G_5 \sim \ell_p^3$, with the Planck length, ℓ_p . This is a specific version of the fluid flow found in [36,37].

The flow in (3) encodes a nontrivial rotation of the fluid and is obtained from the eigenvalue equation for the energy momentum tensor $T_\nu^\mu u^\nu = -\epsilon u^\mu$ of $\mathcal{N} = 4$ SYM theory computed in the large black hole limit (2) after stereographic projection from $\mathbb{R}_t \times S^3$ to $\mathbb{R}^{1,3}$. Initially, the energy density (coloring) is uniformly distributed in rapidity, see left plot in Fig. 1. With time progressing, at $\tau/L = 1$, see center plot in Fig. 1, the energy is now concentrated at mid-rapidity and the fluid velocity spirals outward. Finally at $\tau/L = 2$, see right plot of Fig. 1, the energy density splits into two outgoing pieces at mid-rapidity.

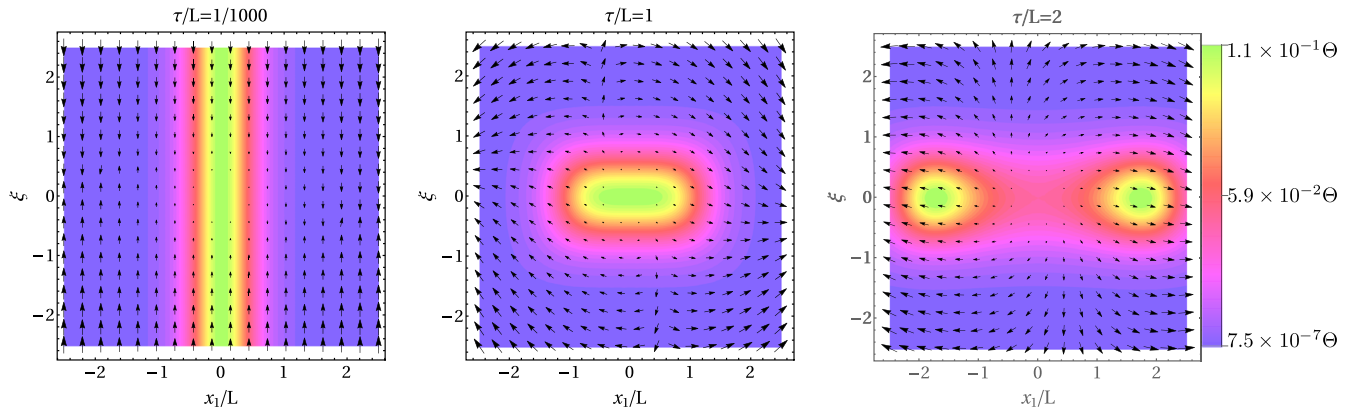


FIG. 1. Flow velocity vectors for different times and $\Omega = 1/2$ in the $x_1 - \xi$ plane (with $x_2 = 0$). The shading corresponds to level sets of the energy density [where Θ is the overall energy scale introduced in (5)]. We have rescaled the energy density by a factor of approximately 250 in the first plot, and 15 in the second plot for the ease of visualization.

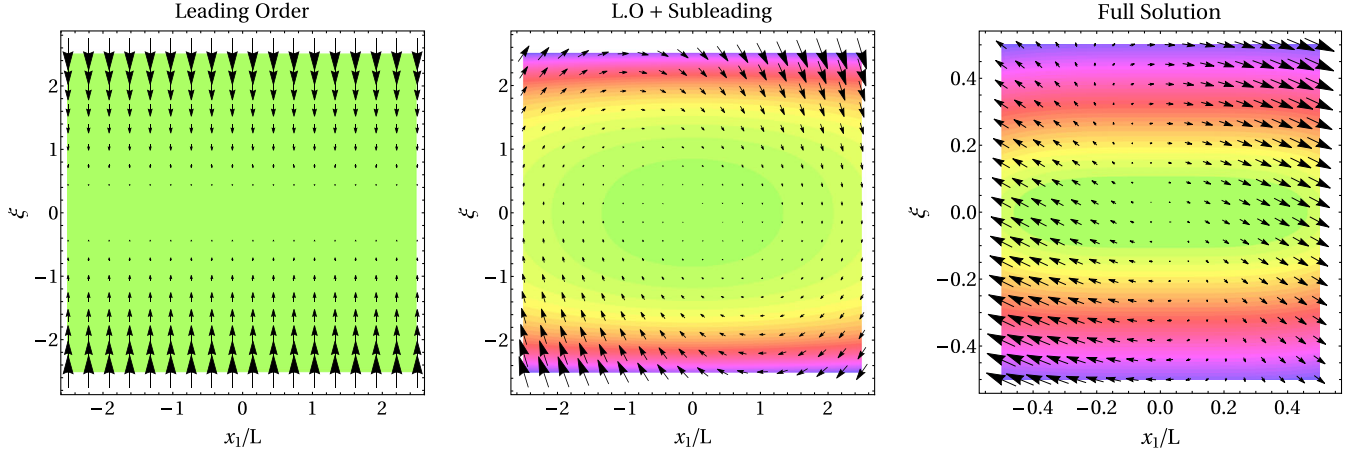


FIG. 2. Flow velocity vectors with $\Omega = 1/2$ in the $x_1 - \xi$ plane (with $x_2 = 0$ and $\tau/L = 1$). *Left*: Leading order. *Center*: Leading order plus subleading order. *Right*: Full solution (center panel of Fig. 1 zoomed in).

One can compute explicitly that the vorticity $\omega_{\text{vor}}^i = \frac{1}{2} \epsilon^{ijkl} u_j \nabla_{[k} u_{l]}$ is nonvanishing for all components. These images demonstrate that this inhomogeneous, time-dependent flow profile has properties which resembles the flow expected for a quark-gluon plasma created in a heavy-ion collision [4,36]. Note that (3) contains also nontrivial rotations in the transverse plane, the $x_1 - x_2$ plane. Moving to Cartesian coordinates, performing a rescaling $x^\mu \rightarrow x^\mu/\alpha$, and subsequently expanding around $\alpha \rightarrow \infty$

$$\frac{u^\mu}{\alpha} = \frac{1}{\sqrt{1 - \Omega^2}} \left(1, \frac{2\Omega x_3}{\alpha L}, \Omega, -\frac{2\Omega x_1}{\alpha L} \right) \quad (6)$$

one can see directly that to leading order the fluid flow is a uniformly boosted fluid, and the first subleading correction is a rotation about the boost direction. The expanded fluid velocity is displayed in Fig. 2 in Milne coordinates. The left most panel displays the leading order contribution, the central panel the leading plus subleading contribution, and the right panel displays the full solution. The full solution displayed is a zoomed in region of the central panel of Fig. 1.

It is important to distinguish this expansion from the large black hole limit in Eq. (2). The fluid flow presented in Eq. (3) is obtained as the leading contribution to the energy-momentum tensor in the large black hole limit. The expansion taken in Eq. (6) is a separate limit meant to understand this leading contribution to the energy-momentum tensor which satisfies the ideal relativistic fluid equations. Furthermore, this expansion will be highly instructive in what follows where we will study the behavior of fluctuations whose momentum and frequencies scale with the horizon radius. These fluctuations will only see the leading contribution in Eq. (6), hence they will see a boosted fluid. However in what follows, we will consider not only this strict large black hole limit, but also the full

MP black hole for which Eqs. (3) and (6) cease to be valid descriptions of the behavior of the dual CFT.

To summarize, in this work, we have performed two holographic calculations in order to determine the hydrodynamic convergence radius:

- (1) A calculation of metric fluctuations around the large black hole metric corresponding to the flow (3), which have frequency and momentum parametrically small compared to the temperature. See hollow symbols in figure 3.
- (2) A calculation of metric fluctuations with arbitrary frequency and momentum around the full rotating black hole metric given in (1) with horizon radius $r_+/L = 100$. See the solid symbols in Fig. 3. If we would expand this result in inverse powers of the horizon radius, the case 1. would be the leading order of this full calculation.

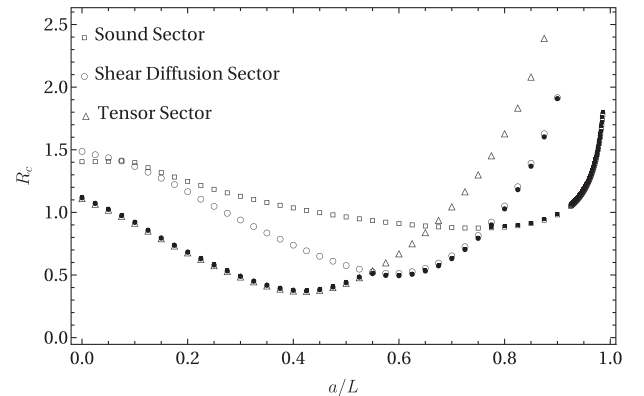


FIG. 3. The convergence radius, R_c , of the hydrodynamic expansion as a function of the angular momentum parameter a/L . Hollow shapes indicate the value in the strict large black hole limit, while solid shapes indicate the value in the full MP black hole with horizon radius $r_+/L = 100$.

IV. HYDRODYNAMIC MODES

In this work, we are interested in hydrodynamic modes, i.e., modes which have a vanishing frequency at vanishing momentum. These hydrodynamic modes on the gravity side correspond to a subset of the quasinormal modes (QNMs) of metric fluctuations around the rotating background (1). Consider the metric fluctuations around (1), which satisfy the linearized Einstein equations [38]

$$\dot{R}_{\mu\nu} = \frac{2\Lambda}{D-2} h_{\mu\nu}, \quad (7)$$

where

$$\dot{R}_{\mu\nu} = -\frac{1}{2}\nabla_\mu\nabla_\nu h - \frac{1}{2}\nabla^\lambda\nabla_\lambda h_{\mu\nu} + \nabla^\lambda\nabla_{(\mu}h_{\nu)\lambda},$$

and $h = h_\mu{}^\mu = h_{\nu\mu}g^{\mu\nu}$. The diffeomorphism-covariant derivatives are defined with respect to the background metric (1). The rotating black hole metric (1) has a spatial $SU(2) \times U(1)$ symmetry such that Wigner-D functions, $D_{\mathcal{K}\mathcal{M}}^{\mathcal{J}}(\theta, \phi, \psi)$, form an orthonormal basis on the S^3 . This is similar to the more familiar spherical harmonics on S^2 . Hence, we choose to expand all metric fluctuations in terms of Wigner-D functions.

The fluctuation equations (7) can be separated into three sectors which decouple because of their different Wigner-charges: the *tensor sector* contains h_{++} with $\mathcal{K}' = \mathcal{J} + 2$, the *momentum diffusion sector* contains h_{+t}, h_{+3} with $\mathcal{K}' = \mathcal{J} + 1$ (h_{++} will decouple in the large black hole limit we will consider), while the *sound sector* contains $h_{+-}, h_{tt}, h_{t3}, h_{33}$ with $\mathcal{K}' = \mathcal{J}$ (h_{++}, h_{+3}, h_{+t} will decouple in the large black hole limit), in radial gauge $h_{\mu r} \equiv 0$. This yields the following form for the vector fluctuations, see [39] for the distinction between \mathcal{K}' and \mathcal{K} (see Supplemental Material [40] for tensor and scalar fluctuation ansatz)

$$\begin{aligned} h_{\mu\nu}^V \equiv & e^{-i\omega\tau} r^2 (h_{++}(r)\sigma_\mu^+\sigma_\nu^+ D_{(\mathcal{J}-1)\mathcal{M}}^{\mathcal{J}} \\ & + 2(h_{+r}(r)\sigma_{(\mu}^+\sigma_{\nu)}^r + h_{+t}(r)\sigma_{(\mu}^+\sigma_{\nu)}^t \\ & + h_{+3}(r)\sigma_{(\mu}^+\sigma_{\nu)}^3) D_{\mathcal{J}\mathcal{M}}^{\mathcal{J}}), \end{aligned} \quad (8)$$

where we chose a convenient frame basis $\sigma^\pm = \frac{1}{2}(\sigma^1 \mp i\sigma^2)$, indicated by the frame index $+$. One may write the Wigner-D functions as

$$D_{\mathcal{K}\mathcal{M}}^{\mathcal{J}}(\theta, \phi, \psi) = e^{-i(\mathcal{M}\phi + \mathcal{K}\psi)} d_{\mathcal{K}\mathcal{M}}^{\mathcal{J}}(\theta), \quad (9)$$

revealing the two Fourier-like exponential factors associating \mathcal{M} with ϕ and \mathcal{K} with ψ .

Each sector can be considered separately, which is reminiscent of the standard procedure considering e.g. sound modes separately from shear diffusion modes in

the nonrotating fluid. Due to time-translation invariance the time-derivative can be replaced by its eigenvalue, the frequency through a Fourier transformation $h_{\mu\nu}(\tau) \propto e^{-i\omega\tau} h_{\mu\nu}(\omega)$: $\partial_\tau h_{\mu\nu} = -i\omega h_{\mu\nu}$, as usual. Similarly, the spatial partial derivatives can be replaced by the eigenvalues of the Wigner-D functions as follows [32–34]

$$\begin{aligned} \partial_+ D_{\mathcal{K}\mathcal{M}}^{\mathcal{J}} &= \sqrt{(\mathcal{J} + \mathcal{K})(\mathcal{J} - \mathcal{K} + 1)} D_{\mathcal{K}-1\mathcal{M}}^{\mathcal{J}}, \\ \partial_- D_{\mathcal{K}\mathcal{M}}^{\mathcal{J}} &= -\sqrt{(\mathcal{J} - \mathcal{K})(\mathcal{J} + \mathcal{K} + 1)} D_{\mathcal{K}+1\mathcal{M}}^{\mathcal{J}}, \\ \partial_3 D_{\mathcal{K}\mathcal{M}}^{\mathcal{J}} &= -i\mathcal{K} D_{\mathcal{K}\mathcal{M}}^{\mathcal{J}}, \end{aligned} \quad (10)$$

where $\partial_\pm = e_\pm{}^\mu \partial_\mu$, $\partial_3 = e_3{}^\mu \partial_\mu$, with orthonormal frame covectors, $\sigma^\pm = \frac{1}{2}(\sigma^1 \mp i\sigma^2)$. So, for example, $\partial_\psi = \sigma_\psi^a \partial_a = \partial_3$ and, thus, $\partial_\psi D_{\mathcal{K}\mathcal{M}}^{\mathcal{J}} = -i\mathcal{K} D_{\mathcal{K}\mathcal{M}}^{\mathcal{J}}$.

As a result of the steps above, the fluctuation equations in a given sector (sound, momentum diffusion, or tensor) depend only on \mathcal{J} , r , and ω (not on \mathcal{M} , \mathcal{K} or on $\partial_\theta, \partial_\phi, \partial_\psi$). The fluctuation equations in the momentum diffusion sector and sound sector are each still complicated sets of coupled differential equations relating three or seven fields, respectively. For illustration, the set of shear diffusion equations is provided in the Supplemental Material [40], Eq. (24). The large black hole limit will simplify them and give rise to a powerful boost symmetry.

V. LARGE BLACK HOLE LIMIT

In the hydrodynamic regime temperature is large, hence, we consider large AdS black holes for which the temperature increases monotonically with the horizon radius r_+ . As a side effect, these black holes are safe from all known instabilities [16,32–34]. We impose this limit on the level of the metric fluctuation equations scaling the frequency and the angular momentum of the fluctuation

$$\omega \rightarrow 2\alpha v r_+/L, \quad \mathcal{J} \rightarrow \alpha j r_+/L, \quad \alpha \rightarrow \infty, \quad (11)$$

simultaneously with the black hole horizon radius and radial coordinate limit given by (2), keeping leading order terms in α . This may be visualized as zooming in on a small patch of the S^3 located at a large radius. Locally, this patch appears noncompact to fluctuations with long wavelengths, i.e., small ν , $j \ll 1$ in the limit (11). In this limit, using standard properties [41], also the third angle, θ , in the Wigner-D function is associated with a combination of eigenvalues $\mathcal{P}(\mathcal{J}, \mathcal{K}, \mathcal{M})$, such that $D_{\mathcal{K}\mathcal{M}}^{\mathcal{J}}(\theta, \phi, \psi) \propto \exp[-i(\mathcal{M}\phi + \mathcal{K}\psi + \mathcal{P}\theta)]$. This closely resembles the Fourier modes $\exp[i(k_x x + k_y y + k_z z)]$ in noncompact Minkowski space and signals the emergence of translation and boost invariance with the effective boundary geometry now being $\mathbb{R}^{3,1} \sim \mathbb{R}_t \times \mathbb{R}^3$.

This leads to the decoupling of several fluctuations, as pointed out above. Furthermore, all fluctuation equations

around the rotating black hole can now be transformed into their form in a black hole at rest (originally stated in [27,28]) by using suitable master fields and the following boost [42] transformation [16]:

$$q^2 = \frac{(a\nu + j)^2}{1 - a^2}, \quad \mathfrak{w}^2 = \frac{(\nu + aj)^2}{1 - a^2}. \quad (12)$$

Specifically, the four coupled shear diffusion equations reduce to a single equation, namely the shear diffusion fluctuation equation in a nonrotating fluid [43], see the Supplemental Material [40]. The sound sector fluctuation equations with (12) reduce similarly to the single master field equation in a nonrotating fluid given in [43].

In summary, the frequencies and momenta of hydrodynamic modes in our rotating fluid can be analytically computed from the known [43] hydrodynamic modes in a fluid at rest. This analytic relation is the Lorentz boost transformation (12).

VI. CRITICAL POINTS AND HYDRODYNAMIC CONVERGENCE

Recent insights gained from the analysis of *critical points of spectral curves* provide a means to determine the radius of convergence of the hydrodynamic series in the linear regime [25,26,44–47]. In hydrodynamics the spectral curve arises from the determinant of a system of hydrodynamic fluctuation equations that encode the hydrodynamic dispersion relations. Hence, the spectral curves are implicit functions of frequency and momentum, i.e., $P(\mathfrak{w}, q^2) = 0$, where $q^2 = \vec{q} \cdot \vec{q}$.

Critical points of spectral curves can be used to determine the radius of convergence of the hydrodynamic gradient expansion in complex momentum space [48,49]. A subset of critical points are branch points from the point of view of complex analysis and, thus, the hydrodynamic dispersion relation of a given mode is not analytic at such critical points. The hydrodynamic expansion is performed about the origin of complex momentum space, $\mathfrak{w} = 0$, $\vec{q} = 0$. Hence, those branch points closest to that origin determine the radius of convergence of the expansion.

However, not all of the critical points of a spectral curve are branch points or any other type of singularity [46]. Hence, in general the radius of convergence based on the nearest critical point is a lower bound for the actual radius of convergence [50]. More precisely, considering the complex \vec{q} -space, the distance of the magnitude-wise smallest critical momentum from the origin, $R_c = |\vec{q}_c|$, is a lower bound on the radius of convergence.

Critical points are defined as those frequencies \mathfrak{w} and momenta \mathfrak{q} which satisfy the constraints

$$P(\mathfrak{w}, \mathfrak{q})|_{(\mathfrak{w}_c, \mathfrak{q}_c)} = 0, \quad \partial_{\mathfrak{w}} P(\mathfrak{w}, \mathfrak{q})|_{(\mathfrak{w}_c, \mathfrak{q}_c)} = 0, \quad (13)$$

where P is a complex-valued function of the complex-valued frequency and momentum $(\mathfrak{w}, \mathfrak{q}) \in \mathbb{C}^2$, and $(\mathfrak{w}_c, \mathfrak{q}_c)$ denotes a discrete set of critical points of the spectral curve. Note, we have used rotation invariance to let the fluctuation travel in one single momentum-direction, \mathfrak{q} . As an example, consider the analytically continued shear diffusion mode defined by the spectral curve

$$P_{\text{shear}}(\mathfrak{w}, \mathfrak{q}) = \mathfrak{w} + iq^2 D(\mathfrak{w}, \mathfrak{q}) + \mathcal{O}(q^4), \quad \mathfrak{w}, \mathfrak{q} \in \mathbb{C}, \quad (14)$$

with the diffusion coefficient D , which in general is a function of the complex momentum. To leading order in derivatives, this encodes the familiar form of the shear mode dispersion relation $\mathfrak{w}(q^2) = -iDq^2 + \mathcal{O}(q^4)$, with all quantities analytically continued to be complex-valued.

For the actual rotating QGP formed in heavy-ion collisions, the hydrodynamic spectral curve P is not known. Thus, we here consider the spectral curve of a rotating $\mathcal{N} = 4$ SYM plasma, in the nontrivial time- and space-dependent equilibrium state shown in Fig. 1, as a substitute for the spinning QGP. In that SYM plasma at rest ($a = 0$) the critical points closest to the origin of complex momentum space were found numerically [25], as an example in the sound channel,

$$\mathfrak{w}_c \approx \pm 1 - i, \quad q_c^2 \approx \pm 2i \quad (\text{sound}). \quad (15)$$

These are calculated from the holographically defined spectral curve $P(\mathfrak{w}, \mathfrak{q}) = 0$, where P is the determinant of all possible metric fluctuations evaluated at the AdS-boundary [26], see the Supplemental Material [40].

VII. CRITICAL POINTS IN THE LARGE BLACK HOLE LIMIT

In the rotating case, the spectral curve can be expressed as $P(\nu, j) = 0$ in terms of the frequency, ν , and angular momentum variable, j . Here, P is the determinant of the metric fluctuations (8) and (33) evaluated at the AdS-boundary. Here we used the fact that the large black hole limit, (2) and (11), implies that the fluctuations depend only on one of the three possible momentum directions, which leads us to consider critical points in one momentum-direction only. This can be rewritten in terms of the nonrotating quantities as $P(\nu, j) = \bar{P}(\mathfrak{w}, \mathfrak{q})$, using (12) in the invertible form $j = \frac{q - a\mathfrak{w}}{\sqrt{1 - a^2}}$ and $\nu = \frac{\mathfrak{w} - aq}{\sqrt{1 - a^2}}$. Thus, the critical point condition in the rotating plasma is given by

$$P(\nu, j) = 0 \Leftrightarrow \bar{P}(\mathfrak{w}, \mathfrak{q}) = 0, \quad (16a)$$

$$\partial_{\nu} P(\nu, j) = 0 \Leftrightarrow \partial_{\mathfrak{w}} \bar{P}(\mathfrak{w}, \mathfrak{q}) + a \partial_{\mathfrak{q}} \bar{P}(\mathfrak{w}, \mathfrak{q}) = 0. \quad (16b)$$

We have used the conditions on the nonrotating spectral curve $\bar{P}(\mathfrak{w}, \mathfrak{q})$, given on the right side of (16a) and (16b), in

order to obtain Fig. 3. This method was verified by a second calculation in which we explicitly calculate numerically the closest critical point in our rotating system using the left side of (16a) and (16b) on the rotating spectral curve $P(\nu, j) = 0$.

The resulting lower bound on the radius of convergence $R_c = |j_c|$ for each sector is given in Fig. 3. In the sound sector (squares), the radius first increases at small angular momentum $a/L < 0.075$, then it decreases to a minimum at $a/L \approx 0.75$. In the shear diffusion sector (circles in Fig. 3), R_c decreases monotonously to a minimum at $a/L \approx 0.6$. This shows that the radius of convergence for the sound (shear diffusion) modes may drop at worst to approximately 60% (35%) of its value in a nonrotating fluid. For large angular momentum beyond their respective minima, $a > a_{\min}$, the radius of convergence of the hydrodynamic expansion increases monotonously and quickly in both, sound and shear sector. The convergence is enhanced for all hydrodynamic modes in a rapidly rotating fluid with $a/L > 0.95$ [51].

VIII. CRITICAL POINTS IN GENERAL

In the large black hole limit the radius of convergence of the hydrodynamic series is the same as that of a boosted fluid. However, as seen in Eq. (6), rotational corrections to the fluid velocity occur away from the strict large black hole limit. Hence to investigate this case we cannot simply keep the leading term in a series around $r_+ \rightarrow \infty$, rather we must include all terms in the equations. Naturally, this suggests how we can systematically move away from the large black hole limit as we can consider solutions for the critical points as a function of the horizon radius. While computationally more complex (see the Supplemental Material [40] where we briefly detail the computational method), the spectral curve and the condition to obtain critical points is still defined as

$$P(\nu, j) = 0 \quad \partial_\nu P(\nu, j) = 0 \quad (17)$$

the major difference now is that we may not use a Lorentz boost as defined in Eq. (12) to relate the frequency, ν , and momentum, j , to their values at rest. Remarkably, however, as seen in Fig. 4, the finite radius corrections have little effect. As already shown in [16], the quasinormal mode spectrum behaves hydrodynamically for black hole radii $r_+/L \approx O(10^2)$. Hence, the large black hole limit, in a sense, is a hydrodynamic limit of the rotating AdS black hole solution. And, it is precisely in this limit that the geometry may be considered to be a boosted black brane. Here we have discovered that the quasinormal modes, which are also critical points, also already behave hydrodynamically for black hole radii $r_+/L \approx O(10^2)$. This is displayed in Fig. 4 where we have plotted the ratio of the radius of convergence of the series at finite r_+ to radius of convergence of the series in the strict $r_+ \rightarrow \infty$ limit. Given

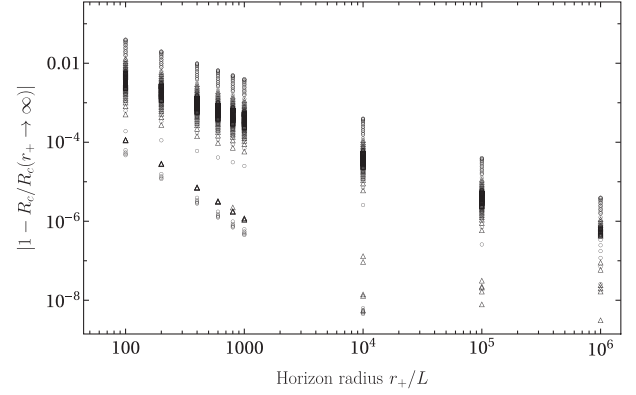


FIG. 4. The deviation of the convergence radius, R_c , of the hydrodynamic expansion as a function of the horizon radius normalized to its value in the large black hole limit. The various points represent different values of the angular momentum parameter a/L . The vertical width of the bands displays the “strength” of rotational effects on the radius of convergence. The plot markers are the same as those used in Fig. 3.

that this quantity is very close to unity, to see the deviation, we consider the difference between this quantity and unity. Appreciable differences (on the percent level) in the radius of convergence only begin to appear for $r_+/L \approx O(10^2)$.

There is, however, a further effect which more severely limits the radius of convergence of the hydrodynamic series away from the large black hole limit. The sectors which can be defined for the MP black hole are defined as tensor, shear, and scalar. The shear sector contains an interaction with the tensor sector and scalar sector contains interactions with the shear and tensor sector (the example of the decoupling of the shear sector is displayed in the Supplemental Material [40]). In the large black hole limit Eq. (2) these interactions are subleading and the sectors decouple. Hence, away from the large black hole limit one must consider the effect of the additional sectors. For example, the spectral curve of the shear sector now contains interactions with tensor sector. While the tensor sector does not contain any modes which can be considered as “hydrodynamic,” it does also contain critical points and these points are closer to the origin in the complex momentum plane. This is reflected in the radius of convergence as displayed as the solid shapes in Fig. 3. While the radius of convergence is still a nonzero finite value, its behavior has changed dramatically as a result of the appearance of the inter-sector couplings.

IX. TRANSPORT COEFFICIENTS

At nonzero angular momentum, transport coefficients split into the ones which measure transport along the angular momentum (longitudinal) and the ones measuring transport perpendicular to it (transverse). This is similar to the case of a charged plasma in the presence of a magnetic field, see [52–55]. Transport coefficients in a fluid at rest

have been extracted from the dispersion relations of the hydrodynamic QNMs [43]. We compute the dispersion relations in a rotating fluid using the transformation (12). We also calculate the QNMs directly in the rotating fluid and confirm that the results agree. For example, when applying (12) the shear diffusion mode dispersion relation in a fluid at rest given in [43], $\mathfrak{w}(\mathbf{q}) = -iq^2/2 + \mathcal{O}(q^3)$, becomes

$$\text{shear: } \nu(j) = -aj - i\frac{1}{2}(1-a^2)^{3/2}j^2 + \mathcal{O}(j^3), \quad (18)$$

where we now set $L = 1$ for ease of notation for the remainder of this section. The sound diffusion dispersion relation is obtained in the same way

$$\text{sound: } \nu(j) = \frac{\pm 1 - \sqrt{3}a}{\sqrt{3} \mp a} j - i\sqrt{3} \frac{(1-a^2)^{3/2}}{(\sqrt{3}-a)^3} j^2 + \mathcal{O}(j^3). \quad (19)$$

From these computations, the following generalized relations are found for the longitudinal diffusion coefficient, \mathcal{D}_{\parallel} , which turns into a damping of a mode now propagating with the speed of shear v_{\parallel} , two modified speeds of sound $v_{s,\pm}$ and two sound attenuation coefficients Γ_{\pm} :

$$v_{\parallel} = a, \quad v_{s,\pm} = v_{s,0} \frac{\sqrt{3}a \pm 1}{1 \pm \frac{a}{\sqrt{3}}}, \quad (20)$$

$$\mathcal{D}_{\parallel} = \mathcal{D}_0(1-a^2)^{3/2}, \quad \Gamma_{s,\pm} = \Gamma_0 \frac{(1-a^2)^{3/2}}{\left(1 \pm \frac{a}{\sqrt{3}}\right)^3}, \quad (21)$$

where for the holographic model the quantities at vanishing angular momentum, $a = 0$, are: $\mathcal{D}_0 = 1/2$, $v_{s,0} = 1/\sqrt{3}$, and $\Gamma_0 = 1/3$. Meanwhile, the two shear viscosities, η_{\perp} and η_{\parallel} were computed in [16] from the corresponding energy-momentum tensor two-point functions, according to the recipe [27,28]

$$\eta_{\perp}(a) = \eta_0 \frac{1}{\sqrt{1-a^2}}, \quad \eta_{\parallel}(a) = \eta_0 \sqrt{1-a^2}, \quad (22)$$

and the shear viscosity at $a = 0$ is given by $\eta_0 = N^2\pi T_0^3/8$. These quantities are related to each other by generalizations of their $a = 0$ Einstein relations

$$\begin{aligned} \mathcal{D}_{\parallel}(a) &= 2\pi T_0 \frac{\eta_{\parallel}(a)}{\epsilon(a) + P_{\perp}(a)}, \\ \Gamma_{\pm}(a) &= \frac{2\eta_{\parallel}(a)}{3(\epsilon(a) + P_{\perp}(a))} \frac{1}{(1 \pm a/\sqrt{3})^3}. \end{aligned} \quad (23)$$

and the bulk viscosity $\zeta(a) = 0$ in our conformal plasma.

X. DISCUSSION

We have computed two main results for rotating $\mathcal{N} = 4$ SYM plasma: (i) The radius of convergence, which quantifies the range of validity of the hydrodynamic gradient expansion, remains nonzero at nonzero angular momentum and eventually increases for fluids with sufficiently large angular momentum (as one approaches extremality in the bulk theory), see Fig. 3. (ii) The values of the shear diffusion, shear viscosity, speed of shear propagation, speed of sound, sound attenuation in the rotating plasma are given analytically as a function of their values in the fluid at rest and as a function of the fluid angular momentum, see Eqs. (20)–(23).

Our analysis reveals new aspects about the domain of applicability of hydrodynamics by determining the fate of the hydrodynamic series in a quantum system undergoing rapid rotation. This is the first time such a study has been performed at nonzero angular momentum, both in non-relativistic and relativistic systems. In fact, different than previous works which employed a constant and uniform equilibrium state in relativistic systems [25,26,44,56–58], here the convergence analysis is performed in a nontrivial time- and space-dependent flow [59]. Assuming our results can be used as a proxy for the rapidly rotating QGP formed in heavy-ion collisions, our work indicates that hydrodynamics remains a good approximation to describe the evolution of this system even when it is subjected to gradients that can be already large enough to spoil the hydrodynamic expansion of its nonrotating counterpart. As such, these results provide useful guidance for future hydrodynamic simulations of heavy-ion collision with nonzero angular momentum.

ACKNOWLEDGMENTS

C. C., M. G. A., and M. K. were supported, in part, by the U.S. Department of Energy Grant DE-SC-0012447. C. C. was also supported, in part, by the Netherlands Organisation for Scientific Research (NWO) under the VICI Grant No. VI.C.202.104. J. N. is partially supported by the U.S. Department of Energy, Office of Science, Office for Nuclear Physics under Award No. DE-SC0021301.

- [1] U. Heinz and R. Snellings, *Annu. Rev. Nucl. Part. Sci.* **63**, 123 (2013).
- [2] P. Romatschke and U. Romatschke, *Relativistic Fluid Dynamics In and Out of Equilibrium*, Cambridge Monographs on Mathematical Physics (Cambridge University Press, Cambridge, England, 2019).
- [3] W. Florkowski, M. P. Heller, and M. Spalinski, *Rep. Prog. Phys.* **81**, 046001 (2018).
- [4] L. Adamczyk *et al.* (STAR Collaboration), *Nature (London)* **548**, 62 (2017).
- [5] F. Becattini and M. A. Lisa, *Annu. Rev. Nucl. Part. Sci.* **70**, 395 (2020).
- [6] W. Florkowski, B. Friman, A. Jaiswal, and E. Speranza, *Phys. Rev. C* **97**, 041901 (2018).
- [7] W. Florkowski, B. Friman, A. Jaiswal, R. Ryblewski, and E. Speranza, *Phys. Rev. D* **97**, 116017 (2018).
- [8] D. Montenegro, L. Tinti, and G. Torrieri, *Phys. Rev. D* **96**, 056012 (2017); **96**, 079901(A) (2017).
- [9] F. Becattini, W. Florkowski, and E. Speranza, *Phys. Lett. B* **789**, 419 (2019).
- [10] W. Florkowski, A. Kumar, and R. Ryblewski, *Prog. Part. Nucl. Phys.* **108**, 103709 (2019).
- [11] K. Hattori, M. Hongo, X.-G. Huang, M. Matsuo, and H. Taya, *Phys. Lett. B* **795**, 100 (2019).
- [12] S. Bhadury, W. Florkowski, A. Jaiswal, A. Kumar, and R. Ryblewski, *Phys. Lett. B* **814**, 136096 (2021).
- [13] D. Montenegro and G. Torrieri, *Phys. Rev. D* **102**, 036007 (2020).
- [14] N. Weickgenannt, E. Speranza, X.-l. Sheng, Q. Wang, and D. H. Rischke, *Phys. Rev. Lett.* **127**, 052301 (2021).
- [15] E. Speranza and N. Weickgenannt, *Eur. Phys. J. A* **57**, 155 (2021).
- [16] M. Garbiso and M. Kaminski, *J. High Energy Phys.* **12** (2020) 112.
- [17] K. Fukushima and S. Pu, *Phys. Lett. B* **817**, 136346 (2021).
- [18] S. Li, M. A. Stephanov, and H.-U. Yee, *Phys. Rev. Lett.* **127**, 082302 (2021).
- [19] A. D. Gallegos, U. Gürsoy, and A. Yarom, *SciPost Phys.* **11**, 041 (2021).
- [20] E. Speranza, F. S. Bemfica, M. M. Disconzi, and J. Noronha, *Phys. Rev. D* **107**, 054029 (2023).
- [21] M. Hongo, X.-G. Huang, M. Kaminski, M. Stephanov, and H.-U. Yee, *J. High Energy Phys.* **11** (2021) 150.
- [22] It is important to note that we do not consider a “spin” hydrodynamic theory, such as the one developed in [19,21], hence we will not attempt to include the spin degrees of freedom in our description.
- [23] H. B. Meyer, *Eur. Phys. J. A* **47**, 86 (2011).
- [24] J. M. Maldacena, *Adv. Theor. Math. Phys.* **2**, 231 (1998).
- [25] S. Grozdanov, P. K. Kovtun, A. O. Starinets, and P. Tadić, *J. High Energy Phys.* **11** (2019) 097.
- [26] S. Grozdanov, P. K. Kovtun, A. O. Starinets, and P. Tadić, *Phys. Rev. Lett.* **122**, 251601 (2019).
- [27] G. Policastro, D. T. Son, and A. O. Starinets, *J. High Energy Phys.* **09** (2002) 043.
- [28] G. Policastro, D. T. Son, and A. O. Starinets, *J. High Energy Phys.* **12** (2002) 054.
- [29] S. W. Hawking, C. J. Hunter, and M. Taylor, *Phys. Rev. D* **59**, 064005 (1999).
- [30] S. W. Hawking and H. S. Reall, *Phys. Rev. D* **61**, 024014 (2000).
- [31] Note that a here is defined with a relative minus sign compared to the a used in [60].
- [32] K. Murata and J. Soda, *Classical Quantum Gravity* **25**, 035006 (2008).
- [33] K. Murata, *Prog. Theor. Phys.* **121**, 1099 (2009).
- [34] K. Murata and J. Soda, *Prog. Theor. Phys.* **120**, 561 (2008).
- [35] I. Papadimitriou and K. Skenderis, *J. High Energy Phys.* **08** (2005) 004.
- [36] H. Bantilan, T. Ishii, and P. Romatschke, *Phys. Lett. B* **785**, 201 (2018).
- [37] A distinct holographic dual of a rotating fluid has also been considered by boosting a static black brane [61].
- [38] R. M. Wald, *General Relativity* (Chicago University Press, Chicago, USA, 1984).
- [39] Note that \mathcal{K}' is the \mathcal{K} -charge of $h_{\mu\nu}$. This is in general distinct from the value \mathcal{K} in the corresponding Wigner-D function, because each σ^\pm carries a \mathcal{K} -charge of ± 1 .
- [40] See Supplemental Material at <http://link.aps.org/supplemental/10.1103/PhysRevD.108.046014> for more details on how the boost symmetry arises in the large black hole limit, and the numerical methods used to compute the critical points.
- [41] N. Tajima, *Phys. Rev. C* **91**, 014320 (2015).
- [42] Furthermore we have checked directly that the transformation given in Eq. (12) is indeed an honest Lorentz boost. Beginning with a Schwarzschild black brane and performing a boost along a given direction one finds the fluctuation equations decouple into sectors which can be written in terms of master variables. The resulting master equations for each sector are directly related to the master equations for a black brane at rest via the transformation in Eq. (12).
- [43] P. K. Kovtun and A. O. Starinets, *Phys. Rev. D* **72**, 086009 (2005).
- [44] B. Withers, *J. High Energy Phys.* **06** (2018) 059.
- [45] M. P. Heller, A. Serantes, M. Spaliński, V. Svensson, and B. Withers, *Phys. Rev. D* **104**, 066002 (2021).
- [46] M. P. Heller, A. Serantes, M. Spaliński, V. Svensson, and B. Withers, *SciPost Phys.* **10**, 123 (2021).
- [47] N. Abbasi and M. Kaminski, *Phys. Rev. D* **106**, 016004 (2022).
- [48] S. Grozdanov, D. M. Hofman, and N. Iqbal, *Phys. Rev. D* **95**, 096003 (2017).
- [49] S. Grozdanov and N. Poovuttikul, *J. High Energy Phys.* **04** (2019) 141.
- [50] The actual radius of convergence may be larger, if it is set by one of the critical points further away from the origin of complex momentum space.
- [51] We note that at vanishing angular momentum, $a = 0$, the convergence radius of the sound mode, $R_c(a = 0) \approx 1.41421$, differs slightly from the convergence radius of the shear diffusion mode, $R_c(a = 0) \approx 1.49131$, in agreement with [25].
- [52] R. Critelli, S. I. Finazzo, M. Zaniboni, and J. Noronha, *Phys. Rev. D* **90**, 066006 (2014).
- [53] J. Hernandez and P. Kovtun, *J. High Energy Phys.* **05** (2017) 001.

- [54] M. Ammon, S. Grieninger, J. Hernandez, M. Kaminski, R. Koirala, J. Leiber, and J. Wu, *J. High Energy Phys.* **04** (2021) 078.
- [55] C. Cartwright, M. Kaminski, and B. Schenke, *Phys. Rev. C* **105**, 034903 (2022).
- [56] N. Abbasi and S. Tahery, *J. High Energy Phys.* **10** (2020) 076.
- [57] A. Jansen and C. Pantelidou, *J. High Energy Phys.* **10** (2020) 121.
- [58] N. Abbasi and M. Kaminski, *J. High Energy Phys.* **03** (2021) 265.
- [59] Often such nontrivial, far-from-equilibrium, states with large gradients are generated numerically and then probed with correlation functions and entanglement entropy, see e.g., [62–67].
- [60] M. Garbiso and M. Kaminski, *J. High Energy Phys.* **10** (2019) 087.
- [61] X. Chen, L. Zhang, D. Li, D. Hou, and M. Huang, *J. High Energy Phys.* **07** (2021) 132.
- [62] P. M. Chesler and L. G. Yaffe, *Phys. Rev. Lett.* **106**, 021601 (2011).
- [63] P. M. Chesler and D. A. Lowe, *Phys. Rev. Lett.* **122**, 181101 (2019).
- [64] C. Cartwright and M. Kaminski, *J. High Energy Phys.* **09** (2019) 072.
- [65] C. Cartwright, *J. High Energy Phys.* **01** (2021) 041.
- [66] C. Cartwright and M. Kaminski, *J. High Energy Phys.* **01** (2022) 161.
- [67] M. F. Wondrak, M. Kaminski, and M. Bleicher, *Phys. Lett. B* **811**, 135973 (2020).